Embedded model control GNC for the Next Generation Gravity Mission

IAC-16,C1,2,3,x35402

EMBEDDED MODEL CONTROL GNC FOR THE NEXT GENERATION GRAVITY MISSION

Luigi Colangelo[a]*, Luca Massotti[b], Enrico Canuto[c], Carlo Novara[d]

[a] *Department of Control and Computer Engineering, Politecnico di Torino, Corso Duca degli Abruzzi 24, Turin 10129, Italy*, luigi.colangelo@polito.it
[b] *Earth Observation Programmes Department – Future Mission Division (EOP-SF), ESA-ESTEC, NL-2200 Noordwijk, The Netherlands*, Luca.Massotti@esa.int
[c] *Department of Control and Computer Engineering, Politecnico di Torino, Corso Duca degli Abruzzi 24, Turin 10129, Italy*, enrico.canuto@polito.it
[d] *Department of Control and Computer Engineering, Politecnico di Torino, Corso Duca degli Abruzzi 24, Turin 10129, Italy*, carlo.novara@polito.it
* Corresponding Author

Abstract

A Next Generation Gravity Mission (NGGM) concept for measuring the Earth's variable gravity field has been recently proposed by ESA. The mission objective consists in measuring the temporal variations of the Earth gravity field over a long-time span, with very high spatial and temporal resolutions.

This paper focuses on the guidance, navigation and control (GNC) design for the science phase of the NGGM mission. NGGM will consist of a two-satellite long-distance formation like GRACE, where each satellite will be controlled to be drag-free like GOCE. Satellite-to-satellite distance variations, encoding gravity anomalies, will be measured by laser interferometry. The formation satellites, distant up to 200 km, will fly in a quasi-polar orbit at an Earth altitude between 300 and 450 km.

Orbit and formation control counteract bias and drift of the residual drag-free accelerations, in order to reach orbit/formation long-term stability. Drag-free control allows the formation to fly counteracting the atmospheric drag, ideally subject only to gravity.

Orbit and formation control, designed through the innovative Integrated Formation Control (IFC), have been integrated into a unique control system, aiming at stabilizing the formation triangle consisting of satellites and Earth Center of Masses.

In addition, both spacecraft must align their control axis to the satellite-to-satellite line (SSL) with micro-radian accuracy. This is made possible by specific optical sensors and the inter-satellite laser interferometer, capable of materializing the SSL. Such sensors allow each satellite to pursue an autonomous alignment after a suitable acquisition procedure. Pointing control is severely constrained by the angular drag-free control, which must ideally zero the angular acceleration vector, in the science frequency band.

The control unit has been designed according to the Embedded Model Control methodology and is organized in a hierarchical way, where the drag-free control plays the role of a wide-band inner loop, and orbit/formation and attitude/pointing controls are the narrow band outer loops. The relevant state equations were converted to discrete time providing the embedded model, a fundamental part of the control unit. The state predictor, control law and reference generator were built on and interfaced to the embedded model.

Simulated results, via a high-fidelity simulator, prove the concept validity and show that the control performances are in agreement with the defined mission requirements. Indeed, the presented control strategy is shown to be capable of keeping the attitude and formation variables stable within the required boundaries, all over the 10-year mission, through a low-thrust authority in the order of a few milli-Newton.

Keywords: Gravimetry; Drag-free; Orbit; Formation; Pointing; Attitude

Acronyms/Abbreviations. Embedded Model Control (EMC), Next Generation Gravity Mission (NGGM), Formation Local Orbital Frame (FLOF), Satellite-to-satellite line (SSL), Measurement bandwidth (MBW), Integrated orbit and Formation Control (IFC), Attitude and Orbit Control System (AOCS).

1. Introduction

Post ESA's GOCE (Gravity field and steady state Ocean Circulation Explorer [1]) and GRACE (Gravity Recovery and Climate Experiment [2]) space Earth gravimetry missions will rely on a formation of free falling 'proof masses' and on the measurement of their distance variations, encoding the gravity anomalies. As a matter of fact, one of the main objectives will be to increase at a greater extent the performance level of gravity missions. Such an ambitious objective can be

achieved by adding a closed-loop formation control in addition to long-distance distributed space systems, as in GRACE, in the order of 100 km distance, but at a lower altitude (300 to 400 km). However, at those altitude ranges, the effects of the Earth atmosphere over the satellites are very severe. Hence, such kind of missions require that each satellite is controlled to be drag-free (up to a certain measurement bandwidth) and completed by an accurate distance measurement system.

Following these main principles, the Next Generation Gravity Mission (NGGM), under study at the European Space Agency (ESA), will consist in a two-satellite long-distance formation, placed in a low near-polar orbit. Each satellite will be autonomously controlled to be drag-free. Concerning the measurement principle, laser interferometry will ensure the satellite-to-satellite tracking and the inter-satellite distance variation measurements.

Consequently, a first set of mission requirements comes from the scientific data elaboration. In this framework, the main requirement concerns the non-gravitational CoM accelerations, as they must be ideally brought to zero. A second set of requirements concerns the orbit and formation control. In this case, the orbit and formation control is designed to counteract the effects of the drag-free control residual, which can make the satellite formation diverging. Finally, the attitude and pointing control system is intended to keep aligned the satellite optical axis and eventually ensure an orbital roll motion for tracking the Sun beam.

The NGGM mission technology is defined as a consequence of the established requirements [3]. Indeed, the drag-free control requires one or more GOCE-class ultrasensitive accelerometers capable of providing linear and angular accelerations. In addition, the formation control requires both a global navigation satellite system (GNSS), in order to materialize the relative satellite position, velocity, and the formation frame, and an inter-satellite link (ISL). As a design choice, all the control functions are actuated by an electric propulsion assembly, able to provide a few milli-Newton thrust level. Finally, satellite-to-satellite mutual alignment variations are measured via an inter-satellite laser interferometer and specific optical sensors.

The approach adopted in the AOCS design for the NGGM mission is based on the Embedded Model Control (EMC) design methodology [4, 5], which calls for a hierarchical and multi-rate control unit around the real-time internal model of the satellite controllable dynamics. This internal (or embedded) model describes the controllable dynamics and the disturbance dynamics. The disturbance dynamics model is in charge of estimating a wide range of unknown model errors as drag-free residuals, parametric uncertainties, cross couplings, and neglected non-linearities.

This paper focuses on the AOCS design principles for the science phase of the NGGM mission. One of the most relevant contributions of this paper is the definition of all the NGGM AOCS architecture control functions within the unified framework of the EMC design methodology. Specifically, for the orbit and formation control, this is enhanced via the definition of an innovative integrated orbit and formation control (IFC) architecture [6]. Such formulation is based on the definition of a peculiar formation reference frame (the formation local orbital frame, FLOF) and the formation triangle virtual structure. A further relevant contribution consists in testing through high-fidelity simulations the effectiveness of the proposed control architecture.

This paper starts with some concepts about the NGGM mission requirements and the architecture of the control design. After this brief outline, the paper describes the main principles of the EMC design and the drag-free concept. Further, the formation triangle dynamics model is made explicit, introducing the FLOF frame. The discrete-time (DT) final equations of the drag-free and the formation internal models are provided. As a consequence, leveraging the EMC design, the state predictor and the control law are built on and interfaced to the internal model. In addition, some sketches about the attitude and pointing control and its interface with the angular drag-free control functions are provided. Finally, some preliminary simulated results verify the control performances and the requirements compliance.

2. NGGM Mission Requirements and EMC Control Architecture

In this section some of the main characteristics of the NGGM mission will be addressed as well as the corresponding control requirements. Further, a general overview of the adopted design methodology (EMC) will be provided, together with the AOCS chief design principles.

1.1 Mission characteristics and requirements

Concerning the satellite formation geometry, two suitable formation types have been proposed as good candidates for the NGGM science mission mode: (i) inline, and (ii) pendulum. The inline formation is characterized by two satellites following the same orbital path, with different true anomalies. On the other hand, in the pendulum configuration, the two satellites are placed on two slightly separated but intersecting orbits, having different right ascension of the ascending node. Further, the nominal altitude range spans between 325 and 425 km on quasi-polar inclined orbits, and the orbit period varies among 5.46 and 5.59 ks. Finally, the nominal inter-satellite distance is in the range of 100-200 km. Such a set of orbital features will allow NGGM to provide an all-latitude coverage, short repeat cycles

and a precise gravity signal with a long mission lifetime (up to 11 years, i.e. a full solar cycle).

The NGGM mission concept leverages a two-satellite formation, ideally drag-free and flying as test masses in the Earth gravity field. Such a pair of distant drag-free satellites acts as a sort of gradiometer, with a very long baseline (≈ 200 km). As a matter of fact, such configuration will make NGGM the first free-falling formation mission. Given the distance variation between the two satellites CoM, which is the mission fundamental observable, a gradiometer-like configuration of this kind has been conceived in order to retrieve only the small fraction, within the total distance variation, due to the gravity acceleration (i.e. the Earth gravity field anomalies effect).

Consequently, from the orbit and formation control perspective, such a drag-free formation implies that no stringent requirements apply to the formation control. Indeed, in principle the two satellites, while acting as proof-masses, must be left free to move under the action of the Earth gravity field. However, since the accelerometer errors (e.g. bias, drift) make an ideal drag-free control not possible, a loose orbit and formation control is needed [3].

The Table 1 lists the main requirements driving the control design in the science mode of the NGGM mission. Note that the formation requirements have been split into distance, radial and lateral variations with respect to a nominal circular orbit; expressed as a percentage of the nominal inter-satellite distance. From the sensor perspective, the requirements match the four accelerometers configuration is adopted, coherently with the latest system studies (see also the tests configuration in Appendix A).

Table 1. NGGM mission science control mode: main performance requirements for the AOCS

Performance variable	Bound	Unit
Drag-free control		
Linear CoM acceleration (PSD in MBW)	0.01	$\mu m/s^2/\sqrt{Hz}$
Linear CoM acceleration	1	$\mu m/s^2$
Angular CoM acceleration (PSD in MBW)	0.01	$\mu rad/s^2/\sqrt{Hz}$
Angular CoM acceleration	1	$\mu rad/s^2$
Orbit and Formation Control		
Formation Distance Variation	5	% (distance)
Formation Lateral Variation	1	% (distance)
Formation Radial Variation	2	% (distance)
Attitude and Pointing Control		
Satellite X-axis pointing along the SSL	2	$\mu rad/\sqrt{Hz}$
Satellite X-axis roll along the SSL	2	mrad

All the requirements above in Table 1 refer to the Scientific Mode (SCM), in which the measurements needed to obtain the scientific product are performed.

This control mode provides fully drag-free environment, formation flying control, optical link between satellites, and orbit control (by ground or autonomous). The science control mode is the last of a series of control modes, starting from the satellites separation from the launcher, and through a mode transition logic based on some monitoring variables. However, the science mode is the fundamental structure on which several control functions of the higher modes are based.

1.2 The Embedded Model Control

The EMC rationale encompasses three model classes to describe the uncertainty affecting the models [4]. The term plant refers to the real system to be controlled (the NGGM spacecraft formation), whereas the digital control unit refers to the NGGM AOCS in charge of orbit, formation and attitude control. The word model corresponds to different classes: (i) the fine model is the more refined, (ii) the design model is a discrete-time simplification formulating the uncertainty class, (iii) the embedded model implements the design model into the control unit. The fine or truth model surrogates the spacecraft system and environment (shortly the plant) and may be a mix of code and hardware. For the purpose of this study, the fine model is written and coded as a mix of continuous-time (CT) and discrete-time (DT) state equations (high-fidelity numerical simulator).

The design model is the DT conversion of the fine model. In this case, the whole dynamics from command to measurement is split into a controllable dynamics, whose states must be included in the embedded model, and into a neglected dynamics, that accounts for the parasitic dynamics outside the EM. The controllable dynamics is completed by three kinds of disturbance signals: (i) known interactions that are not essential to ensure controllability, (ii) unknown interactions that account for the parametric uncertainty, (iii) unpredictable disturbances, to account for unpredictable causes (causal uncertainty).

Finally, the embedded model is the real-time instantiation of the design model inside the control unit. To this end, the neglected dynamics is dropped and the unknown interactions are considered part of the partly unpredictable disturbance. This means that no parameter estimation is done, unlike adaptive control.

Thus, the Embedded Model Control methodology implies the design of an internal model (Embedded Model) coded into the control unit and running in parallel with the plant. The Embedded Model is made up by two main building blocks. Indeed, the controllable dynamics of the plant (spacecraft) is completed by a disturbance dynamics model.

It is interesting to remark that EMC allows us to treat all the wide range of unmodelled dynamics, non-linear effects, and parameter uncertainties as disturbances, collocated at the command level, which

can be estimated and rejected. This disturbance dynamics, being purely stochastic and parameter-free, aims at estimating all these non-modelled effects. The disturbance dynamics is driven by a noise vector

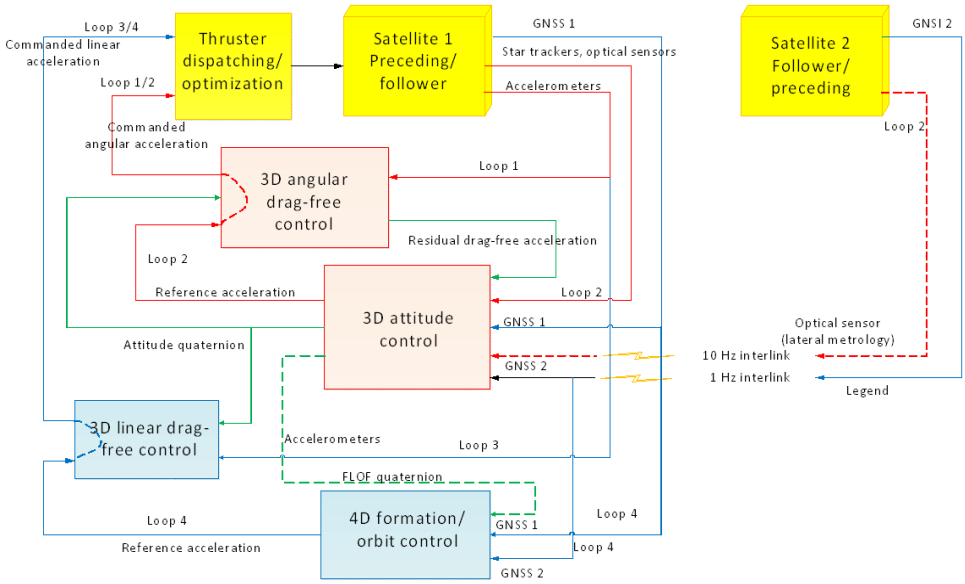

Fig. 1. Higher-level block diagram of the AOCS architecture for the NGGM science mode

playing the role of a disturbance input, to be real-time retrieved from the model error (plant output less model output) by means of a suitable noise estimator (NE). The union of the EM and the NE represents a state predictor, affected by some prediction errors (see, for instance, the orbit and formation predictor in Figure 3).

This disturbance or uncertainty dynamics makes possible to estimate and then reject through the control law all the model errors, neglected or un-modelled dynamics, parametric uncertainties et cetera. Therefore, the embedded model control technique fully solves the typical modelling problems through a simple but effective disturbance estimation dynamics. Hence, one of the main advantage consists in leveraging a simplified LTI internal model but, at the same time, directly rejecting the perturbations from the LTI model, reducing the required thrust level and fuel consumption.

As a property of the EM, all the state variables, forced either by command, or noise, must be observable from the model output. By tuning the eigenvalues of the closed-loop system dynamics, the stability of the state predictor versus the neglected dynamics is achieved.

In addition, starting from the operator target, a reference generator provides the reference trajectories for command and controllable states.

Finally, the control law is composed by three terms: the nominal command, the feedback, and the disturbance rejection.

Control requirements in Subsection 1.1 are formulated through reference values (or time profiles) of the model variables, corrupted by a certain tracking error, whereas the error fluctuation is bounded as in Table 1, in terms either of absolute maximum value or in terms of a spectral density bound within the scientific measurement band ($MBW = \{1mHz \leq f \leq 0.1Hz\}$).

1.3 Control design principles

Given the EMC AOCS design, the main driving principles [6, 7] are:

Integrated orbit and formation control (IFC) The orbit and formation control design is driven by an innovative approach to multi-satellite formation and orbit control based on the integration of orbit and formation dynamics and control through the formation triangle concept, as per Figure 2. As a matter of fact, such modelling idea leads to new CW-type equations (see [6] and Section 4).

Frequency coordination Drag-free control and the formation control are actuated at different frequency bands. This is deemed necessary in order to prevent any possible interference among the inner/outer loops control functions and to coordinate properly the several tasks of the control design.

Multi-hierarchical control The control tasks are carried out via a multi-hierarchical control design (see Figure 1). Indeed, the integrated orbit and formation control is an outer loop which provides the long-term reference accelerations to be tracked by drag-free control.

Attitude and formation decoupling Also favoured by the EMC disturbance dynamics model and due to a microrad alignment between the control frame and the FLOF frame, since the early mission phases, the two frames can be confused. Nevertheless, some coupling

still persists at certain extent in the thruster dispatching algorithm, due to the very limited thrust authority (few milli-Newton as a baseline).

Coordinate decomposition applies to all the control blocks, in Figure 1. For instance, drag-free control is decomposed into six independent SISO (single-input-single-output) loops, taking advantage of the stochastic disturbance dynamics. Specifically, concerning the attitude and pointing, the coordinate decomposition (roll, pitch and yaw) relies on the assumption of small (order of mrad) estimation and tracking errors, since the early mission phases. Nevertheless, the formation embedded model is not completely decoupled, because of the interactions between altitude and distance, in the same ways as longitudinal and radial coupling in Hill's equations.

3. Linear and Angular Drag-free Control

In this section, the main focus will be on the drag-free control, both linear and angular.

Drag-free linear control aims at making the satellites orbit only affected by the local gravity. Therefore, the satellite formation is ideally only subject to differential accelerations due to gravitation, which are revealed by the inter-satellite distance fluctuations. Notwithstanding some secular (low frequency) residual accelerations will affect the satellites orbit, due to the accelerometer errors (bias, drift, et cetera). On the other side, angular drag-free control aims at zeroing all the disturbance torques; including gyro, gravity gradient and aerodynamic torques. Both the commanded force and torques are actuated by a thruster assembly.

Given the impossibility of a perfect drag-free condition, due to the accelerometer errors above mentioned, formation and attitude controls are needed.

From the system perspective, each drag-free satellite, according to the accelerometer concept [8], embarks in a proper cage free-falling masses. In addition, an active suspension system, after performing initial centering after launch, keeps the masses centered in the cage. As a consequence, by measuring the suspension force, it is possible to retrieve a measurement of the non-gravitational forces acting on the satellite, which can be directly cancelled by thrusters commanded by a drag-free control.

The ideal drag-free requirement, both concerning the linear and the angular case, is to zero the residual accelerations in the selected MBW. Outside this frequency interval the requirement may be relaxed in order to accommodate the formation and attitude control authorities.

Drag-free control is actuated separately on each satellite of the NGGM formation. By considering a single satellite, the EMC allows each component to be controlled separately, leading to six decoupled scalar drag-free controls for each spacecraft (three for the linear and three for the angular case).

The Embedded Model (EM) includes a dynamics model of the disturbances and the unmodelled effects affecting the controllable dynamics, driven by arbitrary unknown signals. Such a disturbance estimation model is designed based on experimental data and literature about thermosphere density and experimental thruster noise. Specifically, the studies made during the ESA GOCE mission [8] suggest how a combination of white noise (accounting for the thruster noise), and a first and second-order random drift (modelling thruster noise and aerodynamic forces) is a reliable stochastic model for the class of the expected time realizations.

As a consequence, according to the Embedded Model Control methodology, a ninth-order stochastic disturbance dynamics (third order for each axis) driven by a 12th-dimensional bounded noise vector $\mathbf{w}_d$ allows us to account reliably for the high frequency spectral density of drag, thruster noise and accelerometer bias/drift [6]. The final DT model, from sensor to actuator dynamics, which is embedded in the control unit, is

$$\begin{aligned}\mathbf{x}_a(\mathrm{i}+1) &= \begin{bmatrix} 0 & I & 0 & 0 \\ 0 & I & I & 0 \\ 0 & 0 & I & I \\ 0 & 0 & 0 & I \end{bmatrix}\mathbf{x}_a(\mathrm{i}) + \begin{bmatrix} I \\ 0 \\ 0 \\ 0 \end{bmatrix}\mathbf{u}_a(\mathrm{i}) + I_4\mathbf{w}_d(\mathrm{i}), \\ \mathbf{y}_a(\mathrm{i}) &= \begin{bmatrix} I & 0 & 0 & 0 \end{bmatrix}\mathbf{x}_a(\mathrm{i}) + \mathbf{e}_a(\mathrm{i}) \end{aligned} \tag{1}$$

where the state vector is $\mathbf{x}_a = \begin{bmatrix} z_a & x_d & s_d & z_d \end{bmatrix}^T$, $\mathbf{u}_a$ is the command, $\mathbf{e}_a$ is the model error (plant minus model output), $\mathbf{w}_d$ is the noise signal driving the disturbance dynamics. The first state of the state vector, z_a in $\mathbf{x}_a$ accounts for a simple delay, i.e. the simplified thruster-to-accelerometer dynamics). Further, the second state x_d is the output of the disturbance estimation dynamics, intended to provide, inter alia, a reliable estimate of the total gravitational effects. Finally, s_d and z_d are the two further states complementing x_d in the third-order stochastic disturbance dynamics, as per [6]. As a consequence, if the total acceleration reads

$$\mathbf{a}(\mathrm{i}) = \mathbf{d}_a(\mathrm{i}) + \mathbf{b}_a(\mathrm{i}) + \mathbf{u}_a(\mathrm{i}), \tag{2}$$

where $\mathbf{d}_a(\mathrm{i}) + \mathbf{b}_a(\mathrm{i})$ is the sum of the total estimated disturbances and the accelerometer secular errors (bias/drift), one can write

$$\mathbf{d}_a(\mathrm{i}) + \mathbf{b}_a(\mathrm{i}) = \mathbf{x}_d(\mathrm{i}) + \mathbf{w}_d(\mathrm{i}). \tag{3}$$

The loop is closed by adding to (1) a static noise estimator, as in standard observers,

$$\mathbf{w}_d(\mathrm{i}) = \mathbf{L}\mathbf{e}_a(\mathrm{i}), \tag{4}$$

where a $\mathbf{L}$ is a 12×3 constant matrix, making the closed-loop dynamics asymptotically stable. The non-zero entries (on the diagonal) of $\mathbf{L}$ are computed by assigning the eigenvalues of the closed-loop system matrix, trading-off stability property vs the desired performance level.

It is worth to notice how in (1) the actuator-to-sensor dynamics is simplified to a first-order dynamics (first row in (1)), as a simple delay. Such a design simplification in the Embedded Model is in line with the GOCE drag-free control [8].

From the control perspective, being the thruster-to-accelerometer dynamics in (1) asymptotically stable, the reference tracking is ensured by only cancelling at the better extent the sum of the estimated disturbance $\mathbf{d}_a(\mathrm{i}) + \mathbf{b}_a(\mathrm{i})$. Therefore, from (3), the control law is

$$\mathbf{u}_a(\mathrm{i}) = -\mathbf{x}_d(\mathrm{i}) + \mathbf{u}_{ref}(\mathrm{i}) \tag{5}$$

According to the drag-free control concept, the former term in (5), i.e. the drag-free command, tends to ideally zero the non-gravitational accelerations, within the selected bandwidth. The second term, $\mathbf{u}_{ref}$, provides the reference command, in the spirit of the above-mentioned hierarchical control (see also Figure 1). Indeed, it generically denotes either the formation or the attitude commands, counteracting the drag-free residuals. As a result, the formulation in (5) refers to the generic hierarchical and frequency-coordinated control law, whereas the outer command $\mathbf{u}_{ref}$ will be detailed in the following sections.

4. The Integrated Orbit and Formation

In this section, the main focus will be on the integrated orbit and formation dynamics and control. For the sake of brevity, the inline formation type, in which the satellites follow the same orbital path with different true anomalies, will be addressed.

4.1 The Orbit and Formation dynamics model

The designed orbit and formation embedded model assumes that the high-frequency forcing accelerations are only due to the gravity periodic components. As a matter of fact, this assumption is due to the high-frequency drag-free control action, able to cancel the short-term non-gravitational accelerations.

In the present design, as soon as the formation distance can be on-board controlled (it requires radio interlink to exchange GNSS data), formation and orbit control are combined into a unique strategy, through the definition of the formation triangle virtual structure (Figure 2 and [6]) and the FLOF perturbations definition. By design, the formation triangle vertices join the satellite CoMs and the Earth CoM. The unified model has been built with respect to a common main frame of reference: the Formation Local Orbital Frame (FLOF, see Figure 2).

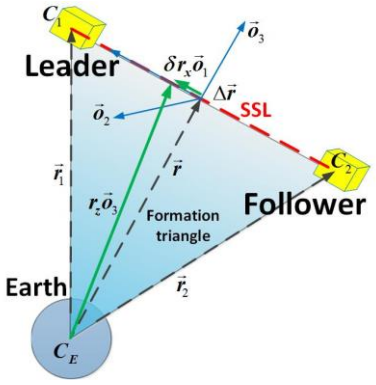

Fig. 2. The formation triangle and the Formation Local Orbital Frame (FLOF)

The three FLOF axes are defined as follows

$$\mathbf{o}_1 = \frac{\Delta\mathbf{r}}{d}, \quad \mathbf{o}_2 = \frac{\frac{\mathbf{r}}{r} \times \mathbf{o}_1}{\left|\frac{\mathbf{r}}{r} \times \mathbf{o}_1\right|}, \quad \mathbf{o}_3 = \mathbf{o}_1 \times \mathbf{o}_2, \tag{6}$$

where $\mathbf{o}_1$ is the satellite-to-satellite (SSL, in Figure 2) direction, $\mathbf{r}$ is the mean formation radius, $\Delta\mathbf{r}$ is the satellites relative position, and d is the inter-satellite distance.

As a consequence, the orbit/formation dynamics is expressed through a combination of Cartesian and angular perturbations (triangle angular rotations), defined through the FLOF frame. Specifically, the three controllable Cartesian perturbations (see Figure 2) are: (i) the distance variation δd , (ii) the formation mean

radius deviation (along the SSL) δr_x, (iii) the mean altitude variation δr_z, defined according to

$$\begin{aligned} \mathbf{\Delta r} &= (\mathrm{d}_{nom} + \delta d), \\ \mathbf{r} &= (r_{nom} + \delta r_z)\mathbf{o}_3 + \delta r_x \mathbf{o}_1, \end{aligned} \tag{7}$$

given the nominal radius r_{nom} and the nominal inter-satellite distance d_{nom}.

The resulting integrated orbit and formation dynamics is expressed through a new set of Clohessy-Wiltshire-type equations, based on the differential equations of the formation triangle perturbations [6].

In order to derive these motion equations, we started from the relative satellite position vectors, and we derived the differential equations of the inter-satellite distance and their derivatives. After that, the formation triangle kinematic equations in terms of the FLOF angular rate and of the angular acceleration, have been obtained, as detailed in [6].

It is worth to notice how the gravity gradient has been kept into account in terms of the spherical gravity term. Indeed, the higher order terms, referred to as gravitational and non-linear, have been considered as external disturbance accelerations. Such a model linearization leverages the Embedded Model Control capability to estimate and reject in the control law all the non-explicitly modelled effects, through the disturbance dynamics.

As a result, the set of differential equations is completed by the six formation degrees of freedom concerning the mean and differential altitude, see [6].

As already mentioned, the rationale behind the orbit and formation control is to counteract the drag-free residuals taking advantage of the wide-band acceleration measurements, while designing a stepwise altitude and distance control sufficiently smooth not to degrade the drag-free residuals. Indeed, given a formation variable, let us say the distance d, it can be decomposed as the sum of three terms: (i) a nominal value d_{nom}, (ii) a secular component d_0, and (iii) a periodic component d_g, due to the gravity field effect. The third component is linked to the scientific product of the mission whereas the second one is due to the accelerometer errors (i.e. bias/drift), preventing a perfect drag-free control. Hence, the orbit and formation control has been conceived as an outer loop aiming at regulating the formation variables to their nominal value, neglecting the periodic component, while trying to zero the secular one.

As a consequence, starting from the above-mentioned set of differential equations, perturbation equations, linearized around the equilibrium point, can be adopted to the purpose of control design. As a matter of fact, such a set of equations, detailed in [6], allows the formulation of the orbit and formation dynamics as a special kind of Clohessy-Wiltshire equations. Specifically, the state vector of our integrated orbit and formation model reads

$$\begin{aligned} \mathbf{x} &= \begin{bmatrix} \mathbf{r}_w & \theta_w & \mathbf{w} \end{bmatrix}^T = \\ &= \begin{bmatrix} \rho_{xw} & \rho_{zw} & d_w & \theta_w & w_x & w_z & w_d & w_y \end{bmatrix}^T, \end{aligned} \tag{8}$$

where the terms w_k are the four normalized formation rate perturbations, while $\rho_{xw} = \rho_x + (w_d - w_z)/2$, $\rho_{zw} = \rho_z + (w_y + w_x)/2$, $d_w = \delta d + \rho_z + 2w_y$, and $\theta_w = d_{nom}\delta\theta - 3\rho_x - 2w_d$ are linear combinations of the formation position perturbation variables. Indeed, $\rho_x = \alpha\delta r_x$, $\rho_z = \alpha\delta r_z$, where $\alpha = d_{nom} / r_{nom}$ is an adimensional scale factor.

The next modelling step leads to the discretization of the equations to implement them within a digital control unit. The discretization step must take into account that the formation control authority should not degrade drag-free requirements as well as the very limited thrust authority. To this aim, a continuous control strategy appears to be useful [6]. As a matter of fact, the orbital rate has been valued as a viable discretisation time step. Hence the IFC command changes each nominal orbit period.

At this point, according to the EMC design, the Embedded Model to be coded directly into the control unit can be built. In the following, for the brevity sake, starting from the complete state vector (8), only the discrete-time final equations of the formation Embedded Model are provided in (9). The embedded model encompasses the controllable model (i.e. the zero-order hold DT formation equations), completed by a purely stochastic and parameter-free disturbance dynamics, to describe the secular components (bias and drift) of the unknown disturbances (see (9)). First of all, to build the controllable dynamics part, starting from the complete state vector in (8), all the uncontrollable variables (namely, the longitudinal perturbation θ_w and the formation rates w_k) have been dropped, since we are only interested in the control of the formation triangle position variables, i.e. $\mathbf{r}_w$ in (8). Then, to the controllable states $\mathbf{r}_w$ we add the states of the stochastic disturbance dynamics, $\mathbf{x}_d$ in (9), to build the integrated orbit/formation Embedded Model, presented in (9). Hence, the linearized secular formation dynamics DT Embedded Model (controllable dynamics plus first-order disturbance dynamics) reads

$$\begin{bmatrix}\mathbf{r}_w\\ \mathbf{x}_d\end{bmatrix}(\mathrm{i}+1)=\begin{bmatrix}A_w & I\\ 0 & I\end{bmatrix}\begin{bmatrix}\mathbf{r}_w\\ \mathbf{x}_d\end{bmatrix}(\mathrm{i})+\begin{bmatrix}B_w\\ 0\end{bmatrix}\mathbf{u}(\mathrm{i})+\begin{bmatrix}\mathbf{w}_r\\ \mathbf{w}_d\end{bmatrix}(\mathrm{i}),$$

$$\begin{bmatrix}\mathbf{r}_w\\ \mathbf{x}_d\end{bmatrix}(0)=\begin{bmatrix}\mathbf{r}_{w0}\\ \mathbf{x}_{d0}\end{bmatrix}\qquad \mathbf{y}(\mathrm{i})=\begin{bmatrix}I & 0\end{bmatrix}\begin{bmatrix}\mathbf{r}_w\\ \mathbf{x}_d\end{bmatrix}(\mathrm{i})+\mathbf{e}_m(\mathrm{i}),$$

$$A_w=\begin{bmatrix}1 & 0 & 0\\ 0 & 1 & 0\\ -12\pi & 0 & 1\end{bmatrix},\quad B_w=\begin{bmatrix}0 & -\alpha/2 & 1/2 & 0\\ \alpha/2 & 0 & 0 & 0\\ 0 & 3\pi\alpha & -3\pi & -2\end{bmatrix}\frac{T_0}{\omega_{nom}}. \tag{9}$$

In (9), $\mathbf{r}_w$ is the controllable state vector (comprising the three states relatively to the distance variations, the mean altitude and formation mean radius deviation). The input variable $\mathbf{u}$ is given in acceleration units. In (9) all the state variables are decoupled except the lateral perturbation pair d_w and ρ_{xw}. $\mathbf{x}_d$ is the disturbance state sub-vector expressing the unknown disturbance dynamics states. Indeed, to describe the secular components (bias and drift) plus the other unmodeled dynamics, three first-order stochastic dynamics were added, as above mentioned. In addition, $\mathbf{w}_r$ and $\mathbf{w}_d$ components play the role of arbitrary, but bounded signals driven by the model error (plant minus model output) $\mathbf{e}_m$. The loop is closed, thus completing the state predictor, by adding to the embedded model a static noise estimator (described by (10)).

$$\mathbf{w}=L\mathbf{e}_m,\qquad \mathrm{L}=\begin{bmatrix}L_x & 0\\ 0 & L_z\end{bmatrix} \tag{10}$$

Finally, the elements of the diagonal matrix $L\in\Re^{6\times3}$ are scalar gains that can be tuned via pole placement, by fixing the closed-loop eigenvalues. This allows a trade-off between fast disturbance prediction and the closed-loop predictor stability.

Extensive simulations [3,6] have shown the IFC model to be satisfyingly robust to the initial orbit perturbations envelope for the science phase of the NGGM mission. Indeed, given the very low thrust level constraining the NGGM control design (few milli-Newtons), stability and drift issues may affect some formation variable in case of a set of initial conditions non optimal for starting the NGGM mission science phase. Specifically, issues of this kind can arise after: (i) poor/missing formation and orbit acquisition, (ii) pre-science control modes transition.

4.2 The Orbit and Formation control law

After the derivation of the orbit and formation state observer, the synthesis of the IFC control law will be addressed in the following. The total linear control action is organized in a hierarchical way, as detailed in (5). The inner loop is the drag-free control (see Section 3); the outer loop is the orbit/formation control (the reference acceleration signal in Figure 1). The actuation time is sampled at the shortest time unit $T=0.1s$ which is imposed by the drag-free control. Therefore, at each control step, the drag-free command is dispatched to the plant, while, at each navigation or orbital step, the IFC part of the command adds up to the drag-free one.

Concerning the IFC, the control algorithms are organized around the above described embedded model (see Section 4). In essence, the IFC control law is the combination of a feedback term and a disturbance rejection term.

On the one hand, the disturbance rejection term is responsible for the embedded model stabilization. Indeed, given the unitary eigenvalues of the disturbance dynamics in (9), the rejection of the estimated disturbances is needed to make the closed-loop system BIBO stable.

On the other hand, the IFC feedback command portion is the result of two combined control strategies. Specifically, the proposed solution relies on a multi-hierarchical structure of the feedback control law able to prevent that the formation rate variables, namely $\mathbf{w}$ in (8), uncontrollable by the low-frequency control of the DT IFC in (9), could affect the controllable variables stability, when closing the loops in some orbital conditions.

Indeed, we have: (i) an orbit and formation stabilization, through the designed low-frequency (orbital) formation position feedback plus (ii) a further stabilizing feedback loop to ensure a proper damping of the formation (rate) variables eventually drifting.

On the one hand, the position feedback operates at the orbital frequency and stabilizes the long-term perturbed dynamics of the formation triangle. Such feedback component leverages the state variables recovered by the state predictor (see (9) and (10), in Section 4), starting from the available measurements.

On the other hand, a formation rate damping control, operating at the time unit of the navigation data, damps suitably the formation rates components which have been found to affect the formation stability. As a further notice, this rate damping control loop is directly fed by the formation rates measurements, obtained from the navigation data, without any state predictor.

As a result, the following IFC total control law holds

$$\mathbf{u}_{IFC}(\mathrm{i}) = -B_y^{-1}K_w\mathbf{y}_w(\mathrm{i}) - B_w^{-1}\left(K_r\mathbf{r}_w(\mathrm{i}) + \mathbf{x}_d(\mathrm{i})\right),$$
$$K_w = \omega_{nom}\mathrm{diag}\{\zeta_x, \zeta_z, \zeta_d, \zeta_w\},$$
$$\zeta_d = 2.8e-7, \quad \zeta_x = \zeta_z = \zeta_w = 0,$$
$$B_y = \begin{bmatrix} \alpha & 0 & 0 & 1 \\ 0 & \alpha & 0 & 0 \\ 0 & 0 & 1 & 0 \\ 0 & 0 & 0 & -1 \end{bmatrix}, K_r = \begin{bmatrix} \gamma_x & 0 & 0 \\ 0 & \gamma_z & 0 \\ -12\pi & 0 & \gamma_d \end{bmatrix}, \tag{11}$$

where $\mathbf{y}_w$ are the formation rate variable measurements, $\mathbf{x}_d$ and $\mathbf{r}_w$ are respectively the disturbances to be rejected and the controllable states prediction, both coming from (9). As a matter of fact, the $\mathbf{u}_{IFC}$ control law stands for the reference part of the multi-loop and hierarchical control law, namely $\mathbf{u}_{ref}$ in (5), in the case of the linear control tasks. Further, the tuning of the feedback control action is pursued via the rate $K_w \in \Re^{4\times4}$ and position $K_r \in \Re^{3\times3}$ feedback gains matrices. Finally, the total command is dispatched to the plant through the inverse and the pseudo-inverse matrices, $B_y^{-1} \in \Re^{4\times4}$ and $B_w^{-1} \in \Re^{4\times3}$. Specifically, B_y is the formation rate command matrix, in the complete IFC model whose state vector is (8), and the pseudo-inverse is essential for rejecting exactly the low frequency components of the disturbance vector $\mathbf{x}_d$, acting on the controlled formation variables.

It is worth to notice that a reference part of the command is missing in (11) because the state variables have been defined as perturbations with respect to their reference value.

The choice of the preliminary control gains in (11) was carried out via a pole-placement procedure and then refined in simulation. Specifically, the gain matrix K_r is fixed by assigning the eigenvalues of the closed-loop matrix $A_w - B_w K_r$, being the tracking error in (11) bounded and zero-mean if and only if $A_w - K_r$ is asymptotically stable.

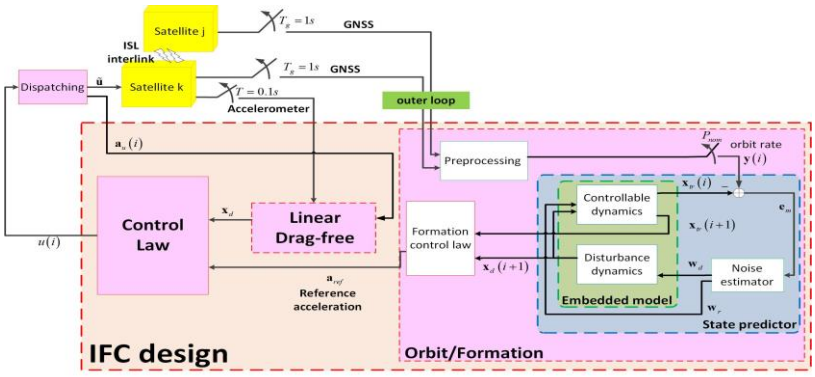

Fig. 3. Overall scheme of the IFC control unit.

Furthermore, the rate feedback portion (through K_w) must be optimised, given the very limited thrust authority constraining the control design. As a result, in a preliminary configuration, only the formation distance rate is proposed to be fed back (gain $\zeta_d \neq 0$). Such preliminary choice, also coming from the most representative and typical inline long-run scenarios, as provided by the preliminary mission studies, was proven to ensure long-term stability as well as a minimum value of the thrust authority.

Figure 3 provides a sketched representation of the IFC control unit block diagram. The embedded model structure is clarified (controllable plus disturbance dynamics), while the noise estimator feedback closes the loop of the formation state predictor. The control law block receives its input both from the embedded model and the navigation sensor. The measurements received by the state predictor are pre-processed in order to filter out the periodic components due to the Earth gravity field.

6. Attitude and pointing rationale

In this section, some notions about the attitude and pointing control design will be provided.

The formation attitude rationale seeks an independent pointing control of each satellite [9]. Such a control action is made possible by disposing of proper optical sensors able to measure the satellite misalignment from the satellite-to-satellite line. As above mentioned, also the pointing control must be coordinated with the angular drag-free control action. Hence, similarly to the linear case, the drag-free sets a

frequency upper-bound to the pointing control action. Notwithstanding, the cancellation of the low-frequency components of the residual acceleration due to the accelerometer drift is instrumental to the NGGM requirements accomplishing. Therefore, a too narrow BW of the pointing control action could result in an insufficient cancellation. As a consequence, a hierarchical and frequency coordinated angular control law will be synthesized, also pointing out some criticalities possibly affecting the current requirements [7].

At the system level, broadly speaking, the attitude control helps to minimize drag-free commands and is responsible to align satellite-to-satellite line to the laser beam (pointing control). As a matter of fact, a pointing control able to align the satellites optical axis is compulsory to measure, via laser interferometry, the inter-satellite distance variations, i.e. the scientific object of the mission. At this proposal, the attitude control, during the mission science phase, leverages a laser beam materialization of the SSL. Each spacecraft is supposed to be equipped with the same laser and optical metrology mechanism respectively launching a laser beam and receiving the beam coming from the companion satellite. Specifically, the optical metrology sensor measures the 2D tilt (pitch and yaw) of the incoming laser beam launched by the companion satellite. Further, the attitude control is actuated by the same propulsion assembly (all-propulsion satellite) responsible for the linear control action and consisting of eight small proportional thrusters capable of a few milli-Newtons thrust. Therefore, there is no pointing mechanism to steer the laser beam [3]. The satellite-to-satellite pointing is characterized by quite strict requirements, as highlighted in Table 1. Conversely, all along the pre-science mission phases, the attitude control is constrained by looser requirements and leverages coarser attitude sensors, like Sun and Earth sensors or star trackers.

The attitude kinematics and dynamics equations used in the control design are based on the definition of a control reference frame, whose origin is in the satellite CoM, in addition to the FLOF frame. The first axis of the control frame is defined by the optical metrology in the motion direction, whereas the second axis is close to the axis of the cross-track accelerometer pair.

The attitude control objective is to reach the alignment of the control quaternion $\boldsymbol{q}_{ck}$, describing the attitude of the satellite control frame with reference to inertial frame, to the FLOF frame quaternion $\boldsymbol{q}_o$ with an accuracy of the order of micro-radians to enable laser interferometry. The wide-band angular drag-free control helps the pointing control action by zeroing the total angular acceleration. The accurate body frame alignment to FLOF allows one to confuse body and FLOF components in the control assumptions. For instance, accelerations can be assumed to be measured in the FLOF frame. Similarly, the alignment of orbital and body frames allows coupling between orbit and attitude (e.g. the non-linear term $h(\cdot)$ in (14)) to be neglected in the control design and treated as a disturbance component.

The attitude model can be described by the vector $\boldsymbol{\theta}_k$ of small 3-2-1 Euler angles $\{\varphi_k, \theta_k, \psi_k\}$ between FLOF and control frame. The pointing control requirements concern mainly the pitch and yaw, while the attitude first component requirement is less stringent. Therefore, the relative attitude quaternion $\boldsymbol{q}_k$, between the control frame and the FLOF frame, reads

$$\boldsymbol{q}_k = \boldsymbol{q}_o^{-1} \otimes \boldsymbol{q}_{ck}, \tag{12}$$

whereas attitude quaternion kinematics is

$$\dot{\boldsymbol{q}}_k(t) = \boldsymbol{q}_k(t) \times \boldsymbol{\omega}_k / 2, \tag{13}$$

where $\boldsymbol{\omega}_k$ is the local satellite angular rate, in control coordinates. The formulation in (13) holds also for the FLOF quaternion, via the FLOF angular rate vector $\boldsymbol{\omega}_o$. The FLOF angular rate can be estimated, provided that some reliable satellite GNSS measures are available. Finally, the satellite dynamics may be described by

$$\dot{\boldsymbol{\omega}}_k(\mathrm{t}) = J^{-1}(\mathbf{M}_c(\mathrm{t}) + \mathbf{M}_d(\mathrm{t})) + \mathrm{h}(\boldsymbol{\omega}_k, \boldsymbol{\omega}_o, \boldsymbol{q}_k)(\mathrm{t}), \tag{14}$$

where J is the inertia tensor, $\mathbf{M}_c$ and $\mathbf{M}_d$ are respectively the command and disturbance torques (in control coordinates), whereas $h(\cdot)$ accounts for the FLOF frame rotation. By pursuing the alignment of control and FLOF frames, the relative attitude quaternion $\boldsymbol{q}_k$ should approach the unit quaternion, while $\dot{\omega}_{ck} \approx 0$ due to the angular drag-free control action.

Consequently, the control design requires a reliable estimation of FLOF quaternion, angular rate and acceleration [9]. According to the EMC methodology, the attitude control unit is based on a discrete-time version of (13) and (14), making the basis of the attitude Embedded Models. Indeed, the attitude and pointing control rationale [9], trough the EMC design, shows how the angular control tasks coordination can be implemented around two Embedded Models, describing

respectively the formation frame (FLOF) quaternion and the spacecraft attitude (relative control frame).

Specifically, the FLOF Embedded Model consists of the quaternion kinematics and of a third order stochastic angular rate model, where the state variables are the angular rate, the angular acceleration and the jerk. The attitude Embedded Model relies on the same equations as the FLOF one, but also the attitude command and the FLOF acceleration are parts of the model.

Concerning the control law, similarly to the total linear command, the angular command $\mathbf{a}_u$ (in angular acceleration units) will be the sum of the drag-free control action $\mathbf{a}_{df}$ and the attitude and pointing one $\mathbf{a}_{ref}$, according to the overall control law expression (5). As a matter of fact, in (15) (first line), $\mathbf{a}_{ref}$ is the reference part of the multi-loop and hierarchical control law, namely $\mathbf{u}_{ref}$ in (5), for what concerns the angular control tasks. The command is sampled at the time unit of the drag-free ($T = 0.1s$) while the attitude command adds up with a bigger sampling step since attitude state predictor and the FLOF predictor operates at the time unit of the navigation data ($T_{gps} = 1s$). Hence the total angular command is:

$$\mathbf{a}_u(i) = \mathbf{a}_{df}(i) + \mathbf{a}_{ref}(i),$$
$$\mathbf{a}_{ref}(i) = -(\mathbf{a}_q(i) + \mathrm{K}_q\,\mathbf{e}_q(i) + \mathrm{K}_v\,\mathbf{e}_{qv}(i))/\mathrm{T}_{gps}{}^2 + \mathbf{a}_o(i). \quad (15)$$

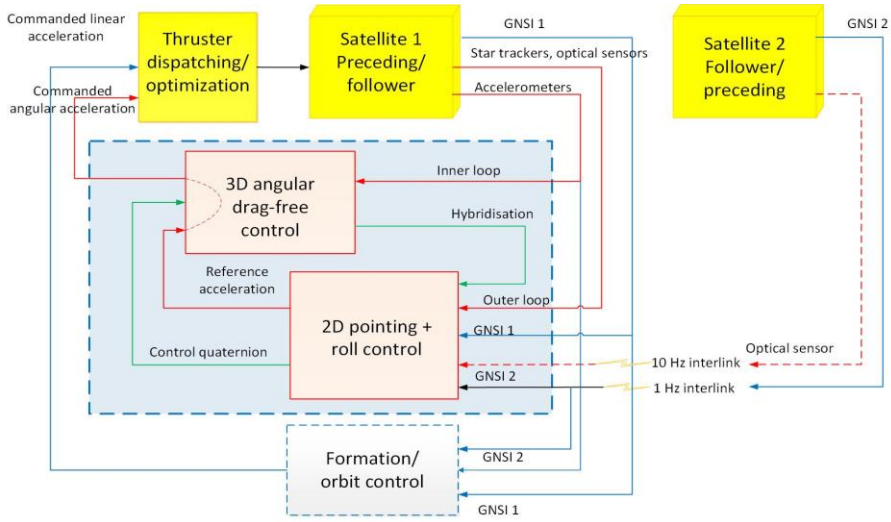

Fig. 4. Overall scheme of the attitude control unit.

In (15) $\mathbf{a}_q$ is the disturbance rejection term (estimated accelerometer bias/drift), $\mathbf{e}_q$ and $\mathbf{e}_{qv}$ the tracking quaternion errors with their the feedback gains K_q and K_v. Finally, $\mathbf{a}_o$ is the reference attitude acceleration command (FLOF acceleration). The EM is completed in both cases with a noise estimator, providing the feedback from the model error to the disturbance states and closing the state predictor loop. However, differently from the formation EM case, the noise estimator cannot be static. Indeed, given a forcing noise vector whose size is less than the state vector, a static noise estimator with its gains cannot stabilize the state predictor (see [4, 9]). Therefore, a first order dynamics noise estimator is implemented.

Finally, the closed-loop gains of the two state predictors must be tuned, trading-off between the several pointing control objectives, according to the rationale illustrated in [7], and based on the frequency analysis of the target pointing bound, compared to the optical sensor noise, and to the doubly integrated accelerometer drift. As a result, we can define three control objectives, along the frequency MBW. First of all, the control action must be able to cancel the accelerometer drift/bias in low frequency band $f < 1mHz$. Secondly, also the attitude sensor noises should be filtered at higher frequencies $(f > 10mHz)$ where they outnumber the accelerometer bound. Thirdly, the stability of the closed-loop state predictor must be guaranteed versus the attitude neglected dynamics.

The rejection of the accelerometer and optical metrology noise requires a careful optimization of the control eigenvalues and may be infeasible, by design. Specifically, the current tests and simulations show how the actual requirements set can be met without great margin (as shown in Figure 9), especially in the medium

frequency band $1mHz < f < 10mHz$, where the contrasting nature of the first two objectives mainly appears.

Finally, Figure 4 depicts a representation of the overall attitude control unit. The hierarchical configuration is clearly visible with the pointing control unit providing the reference command to the angular drag-free block.

7. Simulated results

This section will present some relevant simulated results obtained through a high-fidelity mission simulator including the complete control unit. The first 32 harmonics of the Earth gravity field spherical expansion have been simulated together with an Oersted geomagnetic field model (order 18) and mean solar activity conditions, as per Table 4. From the system perspective, all the sensor and actuator dynamics and noises are active, according to Table 2, Table 3 and [3], [6], [7], [10]. In addition, from the GOCE heritage also realistic misalignment and mounting error matrices have been taken into account in the long-run mission scenario simulation campaign, as summarized in [10]. Each satellite has a nominal mass of 885 kg, and a nominal inertia matrix $J = \mathrm{diag}\{230,1700,1600\}$, as per [7] and [10]. The reference inter-satellite distance has been set to 200 km while the inline orbit configuration has been selected. Parametric uncertainty affects the several sensor parameters as well as thruster assembly parameters.

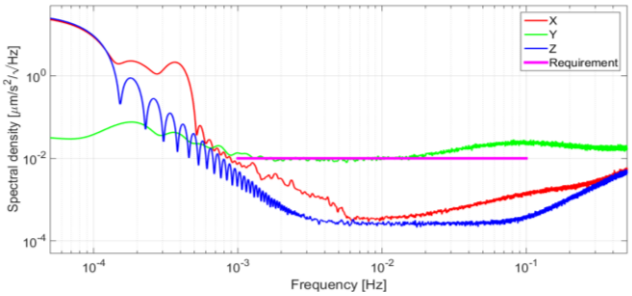

Fig. 5. Simulated PSD of the linear non-gravitational residuals

Figure 5 shows the unilateral spectral density of the linear acceleration residuals versus the performance requirement. The PSD profile is such to respect the requirements. The low-frequency overshoot appears to be linked to the formation transient. Similarly, simulated results showed how the cross-track PSD component (Y-axis, in green in Figure 5) is affected by a very high level of the differential GNSS model noise, thus approaching the requirement bound. In this perspective, there could be room for improvements both at the system and control level.

Figure 6 shows the unilateral spectral density of the angular acceleration residuals versus the performance requirement. The requirement bound is met with some margin. Figure 7 depicts the formation triangle position variables time history (distance variation δ_d, mean altitude r_z and formation mean radius deviation along the SSL r_x) with respect to their reference values. All the variables evolution is within the bound that corresponds to the fractional requirement reported in Table 1.

The simulated total linear command, including both the linear drag-free command and the orbit/formation command is showed in Figure 8. The total longitudinal component (x, in red) includes the longitudinal drag compensation that becomes the largest component when the formation transient vanishes. The behaviour of the total linear thrust components is linked to the choice of the variables to be damped in (11), as well as to the structure of the dispatching matrix, from the integrated formation model to the six components of the force/torque command vector. On the other side, the component along z shows less variation with respect to the x one, also due to the magnitude of the drag affecting the z-axis, which is substantially lower with respect to the longitudinal direction. After the transient, the required thrust authority is well below the level of 3 mN, a value considered compatible with the expected thruster technology level. An overall optimization of the control gains may be beneficial to the improvement of the transient behavior, as shown from the preliminary simulated results, which however was beyond the scope of this study.

Finally, the simulated PSD of the attitude tilt angles is presented in Figure 9. Both satellite pitch and yaw angle PSD meet the requirement bound with some margin. Therefore, the pointing control unit enables the satellites mutual alignment along the SSL line with the desired microrad precision level.

However, as already stated, in the medium frequencies region the margin is quite reduced. This is coherent with the theoretical considerations underlining how, in the critical region $1mHz < f < 10mHz$, the attitude objectives are quite contrasting each other. At this proposal, the star tracker noise can be better filtered than the optical sensors, thus enlarging the margin for $f > 10mHz$ but, as a preliminary conclusion, the low-frequency pointing bound should be enlarged to introduce some margin.

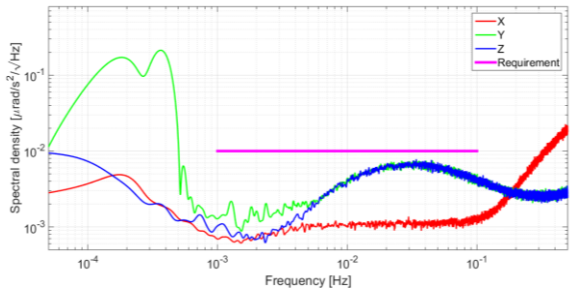

Fig. 6. Simulated PSD of the angular non-gravitational residuals

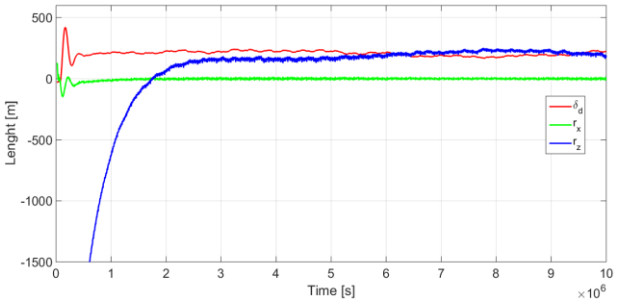

Fig. 7. Formation variable perturbations (formation mean tracking errors)

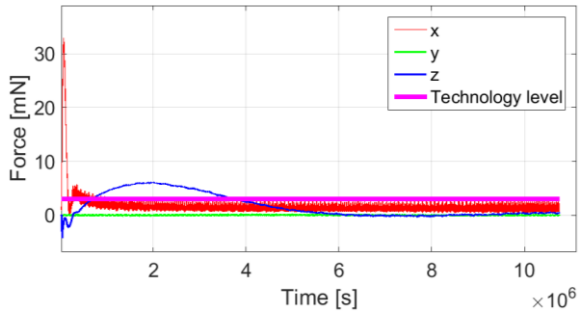

Fig. 8. Simulated total linear command

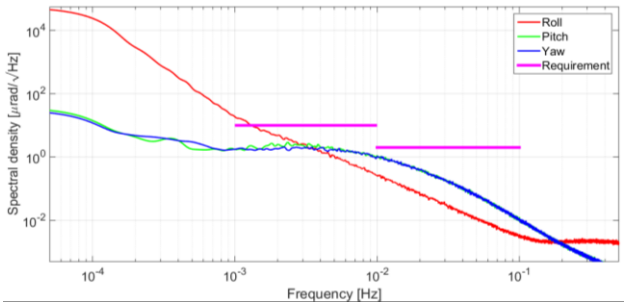

Fig. 9. Simulated PSD of the attitude 2D pointing and roll

8. Conclusions

In summary, we have presented an outline of the AOCS design for the future formation gravity missions, like NGGM under study by ESA. This design was based on the Embedded Model Control Methodology, which employs three model classes to account for the uncertainty affecting models.

Then, the mandatory design in terms of disturbance dynamics, their measurement and rejection for the formation and drag-free control has been described.

The design of the orbit and formation control was tackled through the innovative concepts of formation triangle and the formation local orbital frame (FLOF). This leads to a new set of CW-type equations, suitable to design a formation control which is capable of controlling in an integrated way distance and altitude. An enhanced multi-rate and multi-hierarchical formation control architecture was studied to overcome the possible weaknesses concerning the formation stability in some orbital conditions. Specifically, we envisage a combination of two different control strategies actuating at very different time units. Indeed, the secular perturbations, below the orbital period, are addressed by a low-frequency feedback loop leveraging formation position variables. Then, a further feedback loop was added, involving the formation rate variables and aiming at ensuring their stability.

Also, the rationale and the most relevant aspects of the formation attitude control have been outlined. The formation attitude design was based on the independent pointing control of each satellite, given proper optical sensors measuring the satellite misalignment from the satellite-to-satellite line. Pointing control must be coordinated with the angular drag-free control in a hierarchical way.

Extensive simulated results, run via a high-fidelity simulator, proved the validity of the design concept and showed how the control performance level meets the mission requirements.

Acknowledgements

Part of this research was carried out within the study Next Generation Gravity Mission (NGGM): AOCS Solutions and Technologies study and within the ESA Networking Partner Initiative (NPI) PhD project Laser Metrology Spacecraft Formation (Ref. 4000109653/13/NL/MH) funded by the European Space Agency; Thales Alenia Space Italy (Turin) being the prime contractor.

The first author would like to thank the Italian Space Agency (ASI) and the Space Generation Advisory Council (SGAC) for funding the participation to this conference, within the ASI-SGAC grant 2016 initiative.

The authors would like to thank the reviewers for their helpful suggestions and remarks.

Appendix A (Test parameters)

The tables in this section list the main parameters adopted to test the designed control unit within the high-

fidelity end-to-end mission simulator. Specifically, much attention is devoted to the most relevant sensors, namely the accelerometers and the optical metrology (respectively ACC and OM in Table 2), and the actuators, i.e. the propulsion thruster assembly (TA in Table 3), envisaged for the platform. Finally, some detail about the external atmosphere is provided in Table 4 to complete the information given in Section 7.

Table 2. Long-run simulated test parameters ([3], [6], [7], [10]): sensors*.

Parameter	Unit	Value	Comment
ACC lin. noise	$m/s^2 / \sqrt{Hz}$	$< 9 \cdot 10^{-13}$	X, 4 ACC
	$m/s^2 / \sqrt{Hz}$	$< 1 \cdot 10^{-12}$	YZ, 4 ACC
ACC ang. noise	$rad/s^2 / \sqrt{Hz}$	$< 1 \cdot 10^{-8}$	X, 4 ACC
	$rad/s^2 / \sqrt{Hz}$	$< 3 \cdot 10^{-11}$	YZ, 4 ACC
OM ang. performance	$rad / \sqrt{Hz}$	$1 \cdot 10^{-6}$	
OM lateral performance	$m/\sqrt{Hz}$	$1 \cdot 10^{-2}$	

* frequency performance in MBW

Table 3. Long-run simulated test parameters ([3], [6], [7], [10]): actuators*.

Parameter	Unit	Value	Comment
Overshoot	%	< 5	
Noise	$\mu N/\sqrt{Hz}$	1.2	
Thrust range	μN	50 – 2500	Provisional
Thrust ang. frequency	rad/s	25	2nd order response
Resolution	μN	1	

* frequency performance in MBW

Table 4. Long-run simulated test parameters ([3], [6], [7], [10]): environment.

Parameter	Unit	Value	Comment
Mean solar activity	MJansky/100	95% 140.0 F10	
Geomagnetic index	A_p	18 (≈ 36 nT)	NOAA

References

[1] European Space Agency website - ESA's gravity mission, http://www.esa.int/Our_Activities/Observing_the_Earth/GOCE, (accessed 30.08.16).

[2] GFZ Potsdam website - The GRACE Mission, http://op.gfz-potsdam.de/grace, (accessed 30.08.16).

[3] A. Bacchetta, M. Buonocore, S. Cesare, S. Dionisio, M. Parisch, E. Canuto, B. Girouart, L. Massotti, The Results of the AOCS Solutions and Technologies study for the Next Generation Gravity Mission, AIAA Guidance, Navigation, and Control Conference, AIAA SciTech, (AIAA 2015-1556).

[4] E. Canuto, C.P. Montenegro, L. Colangelo, M. A. Lotufo, Active Disturbance Rejection Control and Embedded Model Control: A case study comparison, In Proceedings of the 33rd Chinese Control Conference, 2014.

[5] E. Canuto, C.P. Montenegro, L. Colangelo, M. A. Lotufo, Embedded Model Control: Design separation under uncertainty, In Proceedings of the 33rd Chinese Control Conference, 2014.

[6] E. Canuto, L. Colangelo, M. Buonocore, L. Massotti, B. Girouart, Orbit and formation control for low-earth-orbit gravimetry drag-free satellites, Proceedings of the Institution of Mechanical Engineers, Part G: Journal of Aerospace Engineering 229(7) 2014 1194-1213.

[7] E. Canuto, L. Colangelo, M. A. Lotufo, S. Dionisio, Satellite-to-satellite attitude control of a long-distance spacecraft formation for the Next Generation Gravity Mission, European Journal of Control, Volume 25, September 2015, Pages 1-16, ISSN 0947-3580.

[8] E. Canuto, Drag-free and attitude control for the GOCE satellite, Automatica, 44(7) 2008 1766-1780.

[9] E. Canuto, L. Colangelo, Angular drag-free control and fine satellite-to-satellite pointing for the Next Generation Gravity Missions, European Control Conference (ECC), Strasbourg, 2014, 3017-3022.

[10] Thales Alenia Space Italy (Turin), Next Generation Gravity Mission AOCS Solutions and Technologies, Ref. SD-RP-AI-0839 Final report, December 2015.